



Cellulose acetate nanofiber modified with polydopamine polymerized MOFs for efficient removal of noxious organic dyes

Esther Eze¹ · Ahmed M. Omer² · Ahmed H. Hassanin^{3,4} · Abdelazeem S. Eltaweil^{5,6} · Mohamed E. El-Khouly¹

Received: 15 November 2023 / Accepted: 19 March 2024 / Published online: 10 April 2024
© The Author(s), under exclusive licence to Springer-Verlag GmbH Germany, part of Springer Nature 2024

Abstract

The need to effectively remove toxic organic dyes from aquatic systems has become an increasingly critical issue in the recent years. In pursuit of this objective, polydopamine (PDA)-binary ZIF-8/UiO-66 (MOFs) was synthesized and incorporated into cellulose acetate (CA), producing ZIF-8/UiO-66/PDA@CA composite nanofibers under meticulously optimized conditions. The potential of fabricated nanofibers to remove cationic methylene blue (MB) dye was investigated. Various analysis tools including FTIR, XRD, SEM, zeta potential, BET, tensile strength testing, and XPS were employed. Results revealed a substantial leap in tensile strength, with ZIF-8/UiO-66/PDA@CA registering an impressive 2.8 MPa, as a marked improvement over the neat CA nanofibers (1.1 MPa). ZIF-8/UiO-66/PDA@CA nanofibers exhibit an outstanding adsorption capacity of 82 mg/g, notably outperforming the 22.4 mg/g capacity of neat CA nanofibers. In binary dye systems, these nanofibers exhibit a striking maximum adsorption capacity of 108 mg/g, establishing their eminence in addressing the complexities of wastewater treatment. Furthermore, the adsorption data fitted to the Langmuir isotherm, and the pseudo-second-order kinetic model. The fabricated nanofiber demonstrates good reproducibility and durability, consistently upholding its performance over five cycles. This suite of remarkable attributes collectively underscores its potential as a robust, durable, and highly promising solution for the effective and efficient removal of pernicious MB dye, in the context of both water quality improvement and environmental preservation.

Keywords MOFs · Nanofiber · Adsorption · Methylene blue · Water treatment · Tensile strength

Responsible Editor: Angeles Blanco

✉ Mohamed E. El-Khouly
mohamed.elkhouly@ejust.edu.eg

- ¹ Nanoscience Program, Institute of Basic and Applied Sciences, Egypt-Japan University of Science and Technology, New Borg El-Arab City, Alexandria, Egypt
- ² Polymer Materials Research Department, Advanced Technology and New Materials Research Institute (ATNMRI), City of Scientific Research and Technological Applications (SRTA-City), New Borg El-Arab City, Alexandria, Egypt
- ³ Department of Textile, Faculty of Engineering, Alexandria University, Alexandria, Egypt
- ⁴ Wilson College Textile, North Carolina State University, Raleigh, NC, USA
- ⁵ Department of Chemistry, Faculty of Science, Alexandria University, Alexandria 21934, Egypt
- ⁶ Department of Engineering, Faculty of Engineering and Technology, University of Technology and Applied Sciences, Muscat, Oman

Introduction

In recent years, the amount of dyes released into the waterways has increased worldwide as a result of increased use in the plastic, textile, pharmaceuticals, etc. (Sağlam et al. 2023; Modi et al. 2022). Among the noxious organic dyes, methylene blue (MB) stands out as one of the most utilized, especially in the textile sector, accounting for 80% of industrial waste (Sağlam et al. 2023; Modi et al. 2022; Fendi and Naser 2018). As known, MB is a soluble organic dye that features a benzene ring with a positive charge and a lone pair electron. This property can lead to adverse reactions in the human body, rendering it susceptible to conditions such as cancer and methemoglobinemia. Moreover, the presence of MB in soil affects plant nutrient absorption, leading to reduced plant productivity (Modi et al. 2022; Fendi and Naser 2018; Eze et al. 2023; Mondal et al. 2016).

In the recent years, various methods such as photocatalysis, membrane filtration, and adsorption have been employed efficiently for wastewater treatment (Abdelfatah et al. 2021;

Tag El-Din et al. 2018; Pi et al. 2018). Given its potential for efficacy, selectivity, and reusability, the adsorption technique represents one of the most promising approaches for wastewater treatment (Abdelfatah et al. 2021; Morcos et al. 2021). Among the utilized adsorbents, metal–organic frameworks (MOFs) have attracted much attention in the wastewater treatment field because of their superior porosity, stability, and surface area, which have garnered significant attention (Katz et al. 2013). Notably, various MOFs, including zirconium, chromium, and zinc-based ones, exhibit high water stability (Katz et al. 2013).

Despite having an impressive surface area and high thermal stability, UiO-66, a zirconium-based MOF with organic linkers and zirconium as a metal ion, showed poor cationic dye removal efficiency (Morcos et al. 2021; Mohammadi et al. 2017; Ruan et al. 2021; Chen et al. 2015). In contrast, ZIF-8 is distinguished by its exceptional chemical and thermal stability, porous structure, substantial surface area, and an abundance of acid–base groups that facilitate ionic interactions (Feng et al. 2016; Zhang et al. 2020; Zhou et al. 2012). However, ZIF-8's hydrophobic nature poses challenges, as it is not readily dispersible in water, affecting adsorption capacity and duration (Zhou et al. 2012; Li et al. 2016; Ding et al. 2019; Luan Tran et al. 2019).

To overcome the limitations of ZIF-8 and UiO-66 in adsorption performance, the fabrication of binary MOFs, with their unique properties and various functional groups on the surface, presents promising materials for the removal of organic pollutants (Zha et al. 2019). Multiple methods, including the addition of hydrophilic molecular linkers and post-modification techniques, have been devised to enhance MOFs' hydrophilicity and functionality (Zha et al. 2019; Eltaweil et al. 2020a; El-Monaem et al. 2022). Altering ligands in MOFs while preserving the overall structure can increase the number of adsorption sites for various target molecules (Mandal et al. 2021; Bepalov et al. 2015). Dopamine (DA) has been widely employed to modify MOFs and other nanomaterials, offering an effective route to enhance their functionality and performance. Dopamine's catechol and amine groups facilitate strong interfacial bonds between dopamine and nanomaterials (El-Monaem et al. 2022; Yang et al. 2021; Chen et al. 2022). Furthermore, dopamine can readily polymerize in an alkaline medium, forming polydopamine (PDA), which enhances material functionality and hydrophilicity (Chen et al. 2022; Liebscher 2019).

However, MOFs in powder form present challenges in terms of regeneration. To address this, the creation of membrane materials with fiber strands through electrospinning offers an effective solution. Electrospinning is a facile method for producing fibrous nanofibers with high porosity and a high surface area-to-volume ratio (Koriam et al. 2022; Paclijan et al. 2021). Nevertheless, nanofibers can suffer from reduced active sites due to pore blockage within

the MOF matrix in the composite. Therefore, the inclusion of polymer additives like polyethylene glycol, which can be easily removed after synthesis to increase pore volume, accelerates adsorption within the nanofiber strands (Chen et al. 2010; Tang et al. 2005). Cellulose acetate, as a naturally occurring polysaccharide, is highly hydrophilic and biodegradable making it suitable for dye adsorption (Elmaghraby et al. 2022; Gopi et al. 2019; Asif and Rafique 2021).

Herein, the polymerization of dopamine in the presence of UiO-66 and ZIF-8 was performed, leading to the synthesis of ZIF-8/UiO-66/PDA composites. Subsequently, we evaluated their efficacy in the removal of MB. Utilizing optimized conditions, we integrated ZIF-8/UiO-66/PDA composites into cellulose acetate (CA) nanofibers to augment the overall performance of CA nanofibers in wastewater treatment. These innovative adsorbents were meticulously engineered to demonstrate exceptional selectivity for the adsorption of cationic (MB). To comprehensively assess their performance, these adsorbents underwent rigorous testing within a complex wastewater matrix.

Materials and methods

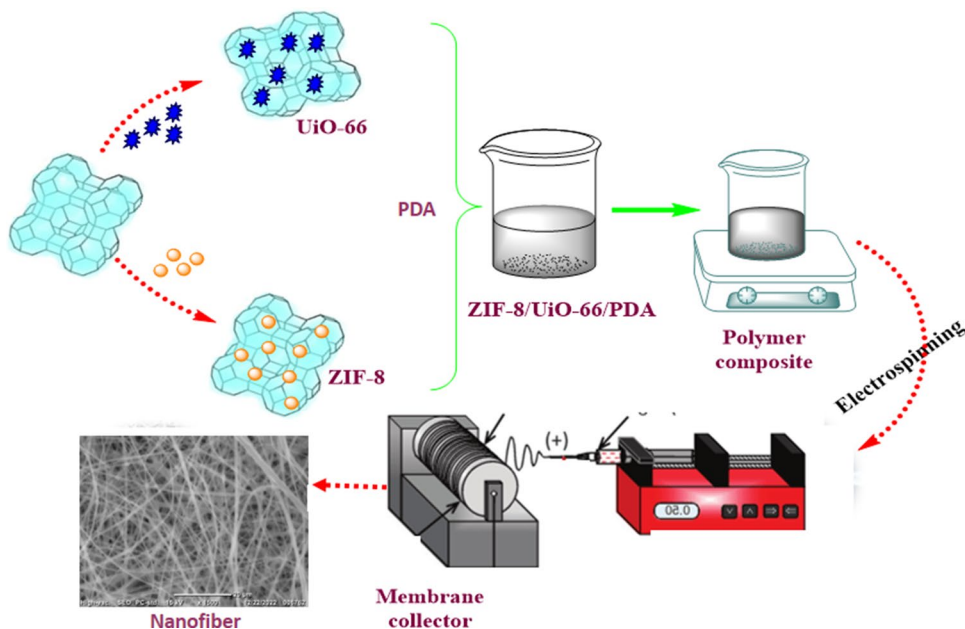
Materials

2-methylimidazole (MeIm; assay 99%), zirconium chloride ($ZrCl_4$; assay $\geq 99.5\%$), zinc nitrate ($Zn(NO_3)_2 \cdot 6H_2O$; assay 98%), and 1,4-benzenedicarboxylic acid (BDC; assay 97%) were purchased from ALPHA Chemie (India). Polyethylene glycol (PEG; Mwt = 200) was purchased from ACROS Organic. Dopamine and acetone (HPLC grade; assay 99.8%) were obtained from Central Drug House (India). N,N-Dimethylformamide (DMF; assay 99.8%) was acquired from Merck (Germany). Methanol (MeOH; assay 99%), Ethanol (assay 98%), and ammonium hydroxide (NH_4OH) were delivered from Sigma Aldrich (Germany). Methylene blue trihydrate (MB), crystal violet (CV), and Congo red (CR) dyes were supplied from Nice Chemicals Pvt. Ltd., (India), and cellulose acetate (Mw = 90,000, DS = 0.7) was purchased from Industrial Corporation (Shanghai, China). All chemicals and solvents were used as received without further purifications.

Synthesis of ZIF-8 and UiO-66 (MOFs)

ZIF-8 (MOF) was prepared according to the reported method (Lee et al. 2015). In the solvothermal method using DMF, 0.67 g (2 mmol) of zinc nitrate hexahydrate ($Zn(NO_3)_2 \cdot 6H_2O$) and 0.167 g (2 mmol) of 2-methylimidazole were dissolved in 50 mL of DMF and stirred vigorously until a clear solution was obtained. The mixture

Scheme 1 Systematic diagram for fabrication ZIF-8/ UiO-66/ PDA@CA nanofiber



was introduced into a 150 mL autoclave with Teflon taped screw cap, and the solution was heated at 140 °C for 24 h in an oven. The product was filtered and washed with DMF and MeOH, then dried at 60 °C overnight. UiO-66 (MOF) was synthesized according to the reported method (Katz et al. 2013). In brief, 0.5825 g of $ZrCl_4$ and 0.4153 g of BDC were dissolved into 50 mL DMF. The mixture was introduced into a 150 mL autoclave with Teflon taped screw cap, followed by the addition of 0.8 mL of HCl, and sonicated for 20 min. The mixture was transferred into a 150 mL autoclave and heated at 120 °C for 24 h. The resultant powder was collected by centrifugation, washed, and dried at 80 °C for 10 h.

Synthesis of ZIF-8/UiO-66/PDA

To synthesize ZIF-8/UiO-66/PDA, a modified method of Eman et al. was used (El-Monaem et al. 2022). In detail, 2.5 mL dopamine hydrochloride was added to 50 mL of distilled water. ZIF-8 was added into the dopamine solution under mechanical stirring followed by the addition of UiO-66. Next, NH_4OH was added to adjust the pH to 8.5. The solution was further stirred for 24 h at 50 °C. Finally, the resultant product was collected by centrifuge after washing severally with distilled water and dried at 70 °C overnight. ZIF-8/UiO-66/PDA composite was synthesized at different ZIF-8: UiO-66 mass ratios of 1:2, 1.5:1.5, and 2:1, which labelled as ZIF-8/UiO-66/PDA-1, ZIF-8/UiO-66/PDA-2, and ZIF-8/UiO-66/PDA-3, respectively.

Fabrication of the electrospun ZIF-8 /UiO-66/PDA @ CA composite nanofiber membrane

Following the preparation methods by Koriem et al. (2022) and Elmaghraby et al. (2022), two solvent DMF/acetone binary solvent mixture (3:1 v/v) was used to produce homogeneous solutions. PEG as an additive was added to the CA solution used to reduce viscosity and to enable the formation of smaller nanofibers (the ratio of CA /PEG was 3:1 w/w). Next, 5 and 10.0 wt% of ZIF-8/ UiO-66/PDA were added to the CA solution to obtain ZIF-8/UiO-66/PDA@CA1 and ZIF-8/UiO-66/PDA@CA2 composite nanofibers. The polymer composite solutions were stirred at room temperature for 24 h. The resultant composites were subjected to electrospinning using a 20 mL syringe pump operating at a flow rate of 1.5 mL/h at 10 cm far from the collector with an applied voltage of 22 kV (Fig. 1). The produced composite nanofiber membranes were collected on a rotating cylinder aluminum collector with a fixed rotation speed of 400 rpm. Scheme 1 Systematic diagram for fabrication ZIF-8/ UiO-66/PDA@CA nanofiber

Characterization

The surface area and pores diameter of the nanofiber were obtained from nitrogen adsorption measurements made at liquid nitrogen temperature, 77 K, and by using the

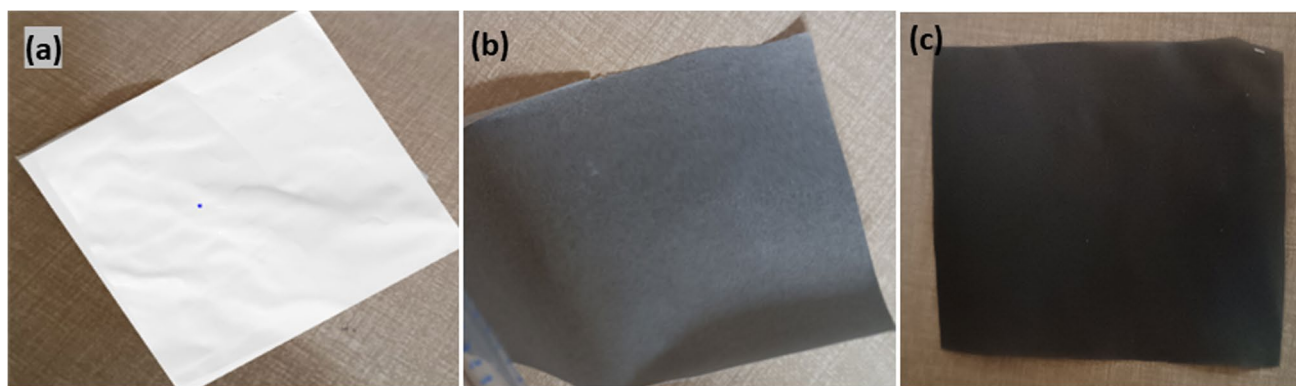


Fig. 1 a CA nanofiber, b ZIF-8/UiO-66/PDA@CA1 nanofiber, and c ZIF-8/UiO-66/PDA@CA2 nanofiber

Brunauer, Emmett, and Teller (BET) equation. The chemical structures of the developed nanofibers were investigated by Fourier transform infrared (FTIR–PerkinElmer Spectrophotometer RXI). To scrutinize the mechanical properties, a universal testing machine (AG-1S, Shimadzu) was employed. Also, the morphological changes were investigated by a scanning electron microscope (SEM, Model JSM-760F) and a transmission electron microscope (TEM, Joel JEM-100CX). Besides, the elemental composition of the nanofibers was verified using X-ray photoelectron spectroscopy (XPS, Thermo Scientific ESCALAB 250Xi VG). Zeta potential (Malvern Zetasizer) was utilized to detect the surface charges.

Batch adsorption studies

Performance of the polymerized MOF composites and nanofibers

To ascertain the best MOF composite, different adsorbents of UiO-66, ZIF-8, ZIF-8/UiO-66/PDA-1, ZIF-8/UiO-66/PDA-2, ZIF-8/UiO-66/PDA-3 were compared by adding 0.02 g of the each in 50 mL MB (25 mg/L) solution for 1 h. The removal of MB dye by CA, ZIF-8/UiO-66/PDA@CA1, and ZIF-8/UiO-66/PDA@CA2 nanofibers composites was carried out using a series of batch adsorption experiments. Known amounts of nanofiber (0.025–0.2 g) were soaked in MB dye (25–200 mg/L). The medium pH was adjusted over the range of 3–10 by HCl (0.1 M) and NaOH (0.1 M) solutions. For each adsorption experiment, samples were collected after time intervals (5–300 min) and filtered regularly, while the remaining MB concentration was assessed using a UV–Vis–NIR spectrophotometer at a wavelength of 664 nm. The adsorption capacity (q)

and the removal ($R\%$) were calculated according to Eqs. 1 and 2 (Elmaghraby et al. 2023):

$$q = \frac{(C_o - C_t) \times V}{m} \quad (1)$$

$$R\% = \frac{(C_o - C_t)}{C_o} \times 100 \quad (2)$$

where, C_o and C_t symbolized initial concentration and concentration at time (t) of MB dye, respectively. $V(L)$ is the volume of MB and $m(g)$ is the composite mass.

Performance of the nanofiber composite for complex wastewater treatment

A variety of tests were conducted to evaluate the membrane's capacity to purify complicated wastewater in binary dye systems. To create simulated complex wastewater, anionic dye (Congo red) and cationic dye (MB) were typically combined. To create the second complex wastewater, two different cationic dyes (MB, CV) were typically combined. The concurrent separation capabilities of the MB, CR, and CV by ZIF-8/UiO-66/PDA@CA nanofiber were tested.

Reusability test

The reusability of a membrane is a criterion to determine the economic benefits of a membrane. Nanofiber membrane regeneration is challenged with getting a suitable solvent to wash out the adsorbate without destroying the structure of the nanofiber. After several tests for regeneration solvent, a mixture of 70% water, 20% 0.1 M HCl, and 10% ethanol was used as a co-solvent at the shortest time of 5 min to regenerate the nanofiber membrane.

Results and discussion

Morphological and physical characterization

TEM

Transmitted electron microscopy imaging of UiO-66 and ZIF-8 produced the following images: UiO-66 exhibits a spherical morphology with an octahedron structure (Fig. 2a), whereas ZIF-8 exhibits a rhombic dodecahedron structure (Fig. 2b). More lumpy particles may be seen in the ZIF-8/UiO-66/PDA polymerized binary MOF (Fig. 2c).

SEM

The microscopic image of the polymerized composite MOF and the surface morphology of each nanofiber spun with various weight percentages of ZIF-8/UiO-66/PDA were both described in Fig. 2. Except for a few aggregates of ZIF-8/UiO-66/PDA in Figs. 2f and g, the image demonstrates

that a free-bead fiber was effectively formed. The average mean diameter increases with increasing the mass of ZIF-8/UiO-66/PDA in the composite, which corresponds to the estimated average diameter (Fig. S1). The rising diameter of the fiber dispersion in Fig. S1 indicates that the MOF composite was successfully impregnated in the CA matrix at various ratios.

XRD

Figure 4a displays the XRD patterns of different CA, UiO-66, ZIF-8, ZIF-8/UiO-66/PDA, and ZIF-8/UiO-66/PDA@CA nanofibers. UiO-66's maxima were seen at 7.35, 8.58, and 25.71°. The ZIF-8 pattern was consistent with the predicted characteristic peaks of ZIF-8 at 7.21, 10.22, 12.63, 14.63, 16.38, and 19.98° (Katz et al. 2013; Wee et al. 2014). The extra peaks with very low intensities may indicate the presence of traces of an additional and unknown phase (Wee et al. 2014). Broad peaks at 20 and 10° are revealed by CA (Korriem et al. 2022). The XRD of ZIF-8/UiO-66/PDA@CA1 nanofibers shows no crystalline peaks of MOFs which

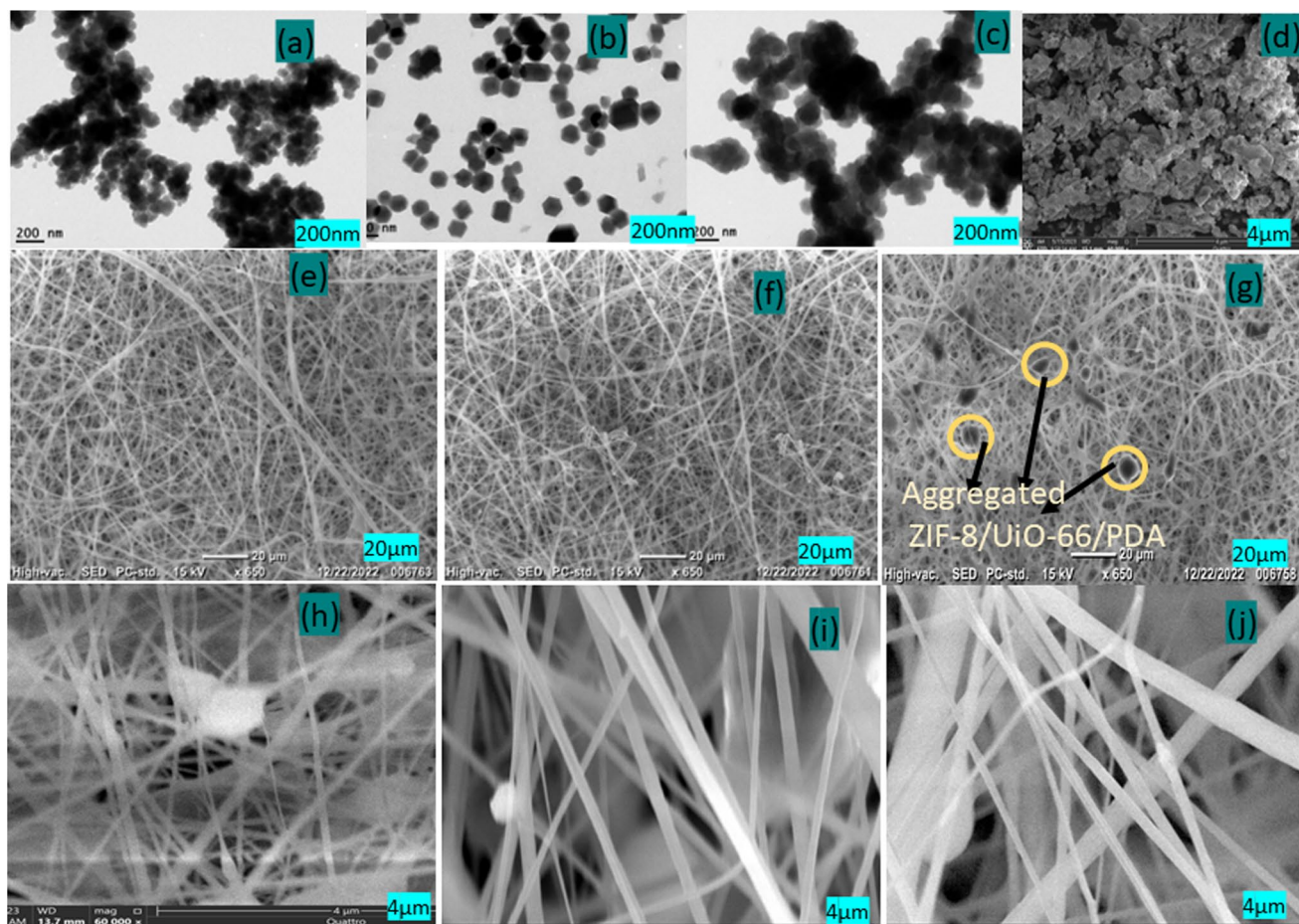


Fig. 2 TEM images of **a** UiO-66, **b** ZIF-8, and **c** ZIF-8/UiO-66/PDA and SEM images of **d** ZIF-8/UiO-66/PDA, **e**, **h** CA nanofiber at 20 μm and 5 μm, **f**, **i** ZIF-8/UiO-66/PDA@CA1 at 20 μm and 5 μm, **g**, **j** ZIF-8/UiO-66/PDA@CA2 nanofibers at 20 μm and 4 μm

might be due to the high dominance of the CA structure; however, an amorphous hump was triggered at 23° . As illustrated in Fig. 3a, the obtained ZIF-8/UiO-66/PDA@CA2 nanofibers have a semi-crystalline structure of the MOF composite with some crystalline peaks of UiO-66 and ZIF-8 located at 8, 10, and 15° and disappearance of some their crystalline peaks in the CA nanofiber matrix (El-Monaem et al. 2022).

FTIR

The FTIR spectra of all composites before adsorption are displayed in Fig. 3b in the region of 4000 to 500 cm^{-1} . The broad absorption band of each composite in the region of 3500 to 2950 cm^{-1} corresponds to the stretching vibration of OH from the carboxylate groups. UiO-66 peaks of 1690 and 1395 cm^{-1} correspond to the symmetrical and asymmetric stretching vibrations of the O-C-O group in the framework. The bands at 737 and 648 cm^{-1} are ascribed to the C-H stretching vibration of the phenyl ring, which are part of the functional groups in the BDC organic linker (Ruan et al. 2021; Zha et al. 2019). The peak at 664 and 455 cm^{-1} is consistent with the symmetric vibration peak of O-Zr-O and Zr(OC) proving the ligands to zirconium metal nodes bond (Katz et al. 2013; Mandal et al. 2021). FTIR spectra of synthesized ZIF-8 have an absorption peak at 2962 , 1600 , 1176 , 992 , and 508 cm^{-1} which correspond to C=N of aromatic imidazole ring; CH_3 of the aliphatic ring of Melm; C=C of the phenyl ring; and N-H and Zn-H which are characteristic absorption peaks of ZIF-8 solids (Chang et al. 2020; Kim et al. 2019). Most of the characteristic peaks of UiO-66 and ZIF-8 reappear on the polymerized MOF composites ZIF-8/UiO-66/PDA showing strong broad peaks of OH and NH (catechol and amine groups of dopamine) stretching at 3500 – 3300 cm^{-1} . FTIR spectrum of ZIF-8/UiO-66/PDA@

CA1 nanofibers shows the same characteristic peaks of CA and ZIF-8/UiO-66/PDA composite with intense OH peaks at 295 cm^{-1} resulting from the added carboxylic group of CA (El-Monaem et al. 2022). ZIF-8/UiO-66/PDA@CA2 nanofibers show no obvious new peaks since the elemental composition remains the same with ZIF-8/UiO-66/PDA@CA1 nanofibers.

BET

The Brunauer–Emmett–Teller (BET) method was used at 77 K to examine the N_2 adsorption characteristics of ZIF-8/UiO-66/PDA, CA, and ZIF-8/UiO-66/PDA@CA2 nanofibers. The N_2 isotherm is shown in Fig. 4a and may be categorized as a type I isotherm indicating a microporous property. The BET surface areas were $341\text{ m}^2/\text{g}$, $5.4\text{ m}^2/\text{g}$, and $14.1\text{ m}^2/\text{g}$ for ZIF-8/UiO-66/PDA, CA, and ZIF-8/UiO-66/PDA@CA2 nanofiber, respectively. From the premises of the obtained value, there was an increase in the surface area of CA nanofiber from 5.4 to $14.2\text{ m}^2/\text{g}$ because of the incorporated ZIF-8/UiO-66/PDA. The total pore volume for ZIF-8/UiO-66/PDA, CA, and ZIF-8/UiO-66/PDA@CA nanofibers were found to be 0.2025 , 0.0349 , and $0.00236\text{ cm}^3/\text{g}$, respectively. The mean pore diameters (Mp) of 24.872 , 10.763 , and 19.7 nm were determined for ZIF-8/UiO-66/PDA@CA, CA, and ZIF-8/UiO-66/PDA@CA2 composites nanofiber mats, respectively (Fig. S2).

Zeta potential

Zeta potential was employed to identify the charges on the surface of nanofibers. The pH of a solution has a direct effect on the charge of a material in an aqueous solution (Večeř and Pospíšil 2012). At a high pH above 6, it tends to be anionic; below pH 6, the material tends to be more cationic. Figure 4b

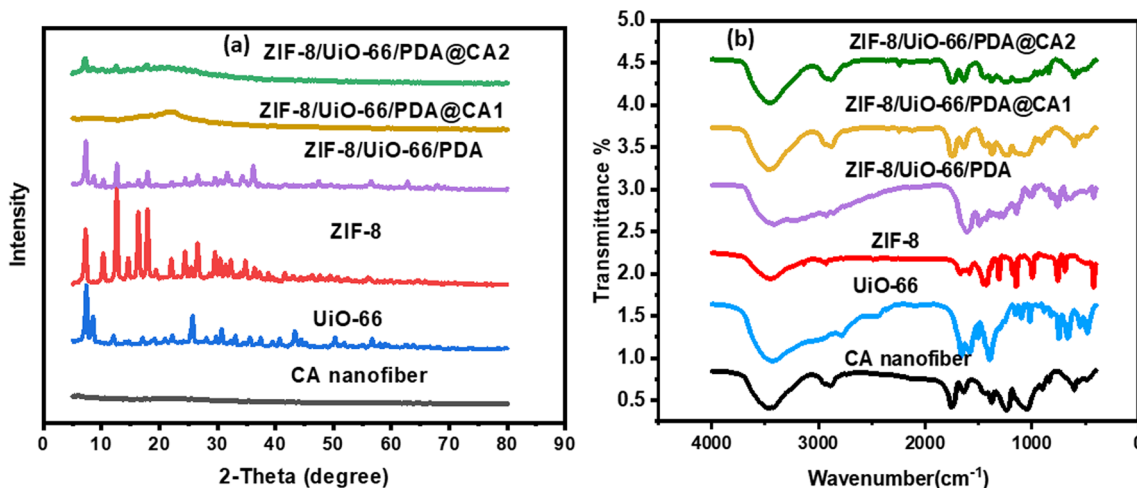


Fig. 3 a XRD and b FTIR spectra of UiO-66, ZIF-8, ZIF-8/UiO-66/PDA, and ZIF-8/UiO-66/PDA@CA nanofibers

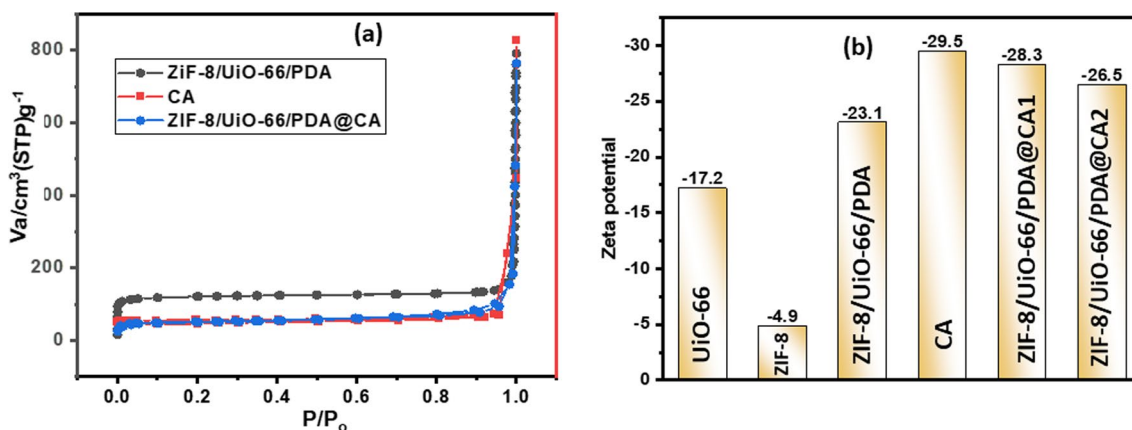


Fig. 4 **a** BET isotherm and **b** Zeta potential for the examined materials

shows the synthesized materials and their zeta potential. The zeta potential values of ZIF-8 and UiO-66 were -4.9 and -17.2 mV. From the obtained results, it is interesting to note that the hydrothermally synthesized ZIF-8 MOF was hydrophobic, and so had limited dispersion in the aqueous medium. Therefore, the potential value for ZIF-8 may not truly define the net potential in a dispersed medium. As anticipated, the polymerization of polydopamine on binary MOF causes a rise in surface charge to -23.1 mV. The potential of the CA electrospun nanofiber was -29.5 mV, which is in line with previously published results (Muqet

et al. 2018; Pottathara et al. 2020). ZIF-8/UiO-66/PDA@CA1 composite MOF reduces the potential of the spun CA fiber to -28.3 mV while ZIF-8/UiO-66/PDA@CA2 nanofibers further reduces the potential to -26 mV.

XPS

The XPS survey scan and spectra of ZIF-8/UiO-66/PDA@CA2 nanofiber are shown in Fig. 5. C1s spectrum (Fig. 5a) points out peaks at 284.06, 285.81, and 289.09 eV which belong to C–C/C–H, C–NH₂, and O–C=O, respectively. In

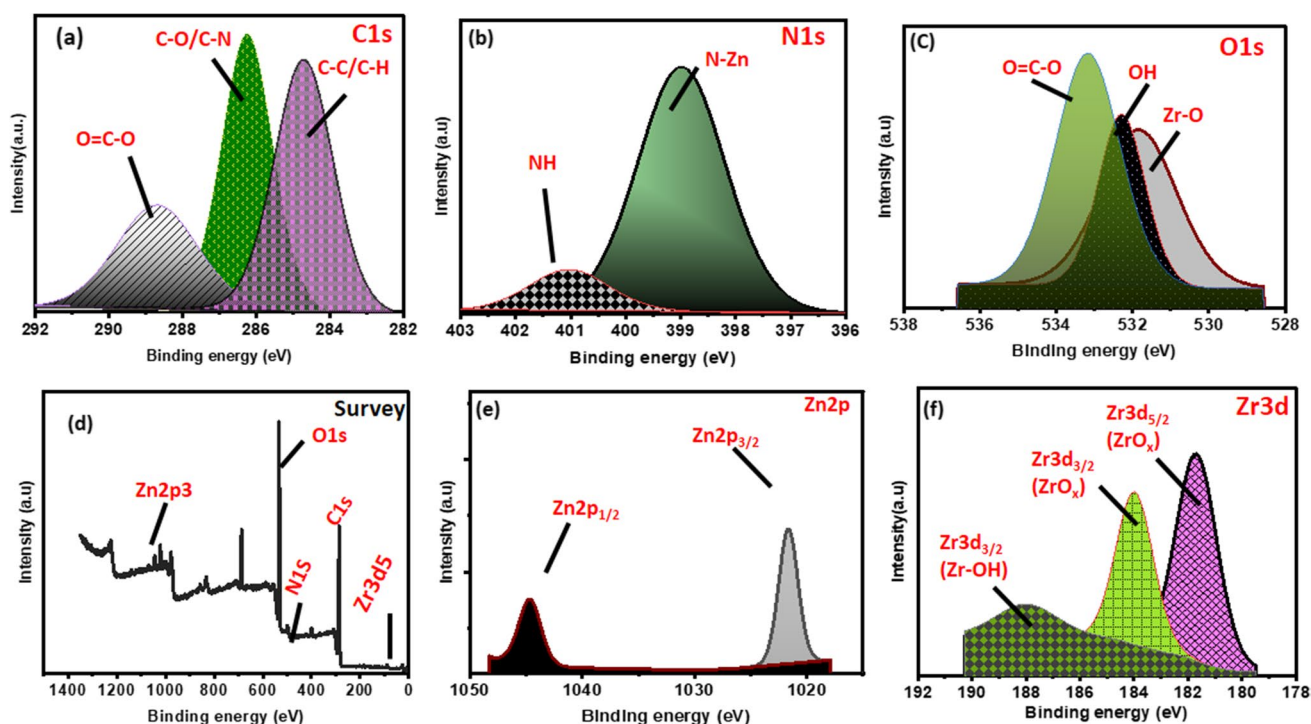


Fig. 5 XPS of ZIF-8/UiO-66/PDA@CA2 nanofibers before adsorption. **a** C1s, **b** N1s, **c** O1s, **d** survey, **e** Zn2p, and **f** Zr3d

the N1s spectrum (Fig. 5), two spectra were observed at 401 and 399 eV which are allocated to NH and N-Zn which are characteristic peaks of dopamine of ZIF-8. The O1s spectrum (Fig. 6c) further reveals oxygen-containing groups such as OH, COO, and C=O at 532.01, 532.76, and 534.54 eV, respectively. Besides, the O1s spectrum further attests to the formation of UiO-66 since the distinguishing peak to Zr-O appeared at 532.14 eV where the formation of ZIF-8 is asserted via N1s spectrum that emerged the discriminative peak to N-Zn at 399.88 eV (El-Monaem et al. 2022; Ayiania et al. 2020). The elements present in each sample are identified as C1s, N1s, O1s, Zr3d, and Zn2p3, with corresponding peaks at 184, 288.74, 399.44, 534.21, and 1021.85 eV, respectively, in the survey diagram (Fig. 5d). The Zn2p_{3/2} and Zn2p_{1/2} spectrum (Fig. 5e) were observed at 1022.09 and 1045.23 eV, which also confirms the presence of ZIF-8 MOF. Furthermore, Zr3d spectrum (Fig. 5f) reveals the signals at 182.48, 184.24, and 188.38 eV which are assigned to Zr3d_{5/2}(ZrOx), Zr3d_{3/2}(ZrOx), and Zr3d_{3/2}(ZrOH), respectively (El-Monaem et al. 2022; Ayiania et al. 2020; Gondal et al. 2017).

Mechanical properties

The mechanical properties of CA, ZIF-8/UiO-66/PDA@CA1, and ZIF-8/UiO-66/PDA@CA2 nanofibers were examined by observing the tensile strength, Young modulus, and elongation as shown in Fig. 6, while the results are summarized in Table 1. It can be observed that values of the Young modulus (131 MPa) and tensile strength (2.8 MPa) of ZIF-8/UiO-66/PDA@CA1 nanofiber are found to be much higher than that of pure CA nanofibers (45 MPa, 1.0 MPa).

This proves that the composite has a positive effect on the mechanical properties of the nanofiber. However, when the ZIF-8/UiO-66/PDA composite increases in ZIF-8/UiO-66/PDA@CA2 nanofiber, it shows a lower Young modulus of 122 MPa and tensile strength of 2.2 MPa compared to ZIF-8/UiO-66/PDA@CA1. On the other hand, the addition of MOF had a negative effect on the membrane elongation. So overall, it can be noticed that by adding MOF, the stiffness of the composite membranes has been significantly increased due to increasing maximum stress and reduction in strain or maximum elongation.

Performance in MB dye removal

Performance of the pristine MOFs and MOFs composite

The adsorptive performance of synthesized MOFs and their composites UiO-66, ZIF-8, ZIF-8/UiO-66/PDA were examined towards the adsorption of MB from an aqueous solution (Fig. 7a) at a shorter time. Their removal (%) results were as follows: ZIF-8 has 21% removal with an adsorption capacity of 12.2 mg/g and UiO-66 has 60% removal with 37 mg/g adsorption capacity. For the polymerized MOFs, among the three different prepared adsorbent representing different ratio of ZIF-8 and UiO-66: ZIF-8/UiO-66/PDA1 composite has 52% removal with adsorption capacity of 32 mg/g, ZIF-8/UiO-66/PDA-2 has 80% removal with adsorption capacity of 49 mg/g, and ZIF-8/UiO-66/PDA-3 with 96% removal and 59 mg/g adsorption capacity. From the obtained data, one can see that ZIF-8/UiO-66/PDA-3 shows superior dye removal. The superior dye adsorption was observed for the MOF composite with a higher amount of ZIF-8. This

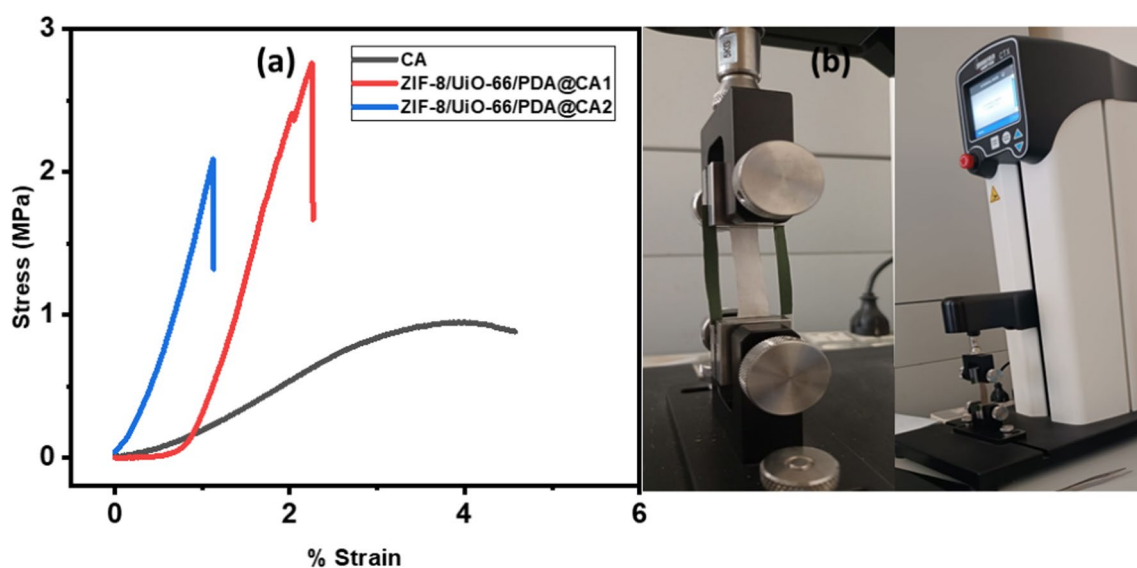


Fig. 6 Stress–strain plot of each type of nanofiber

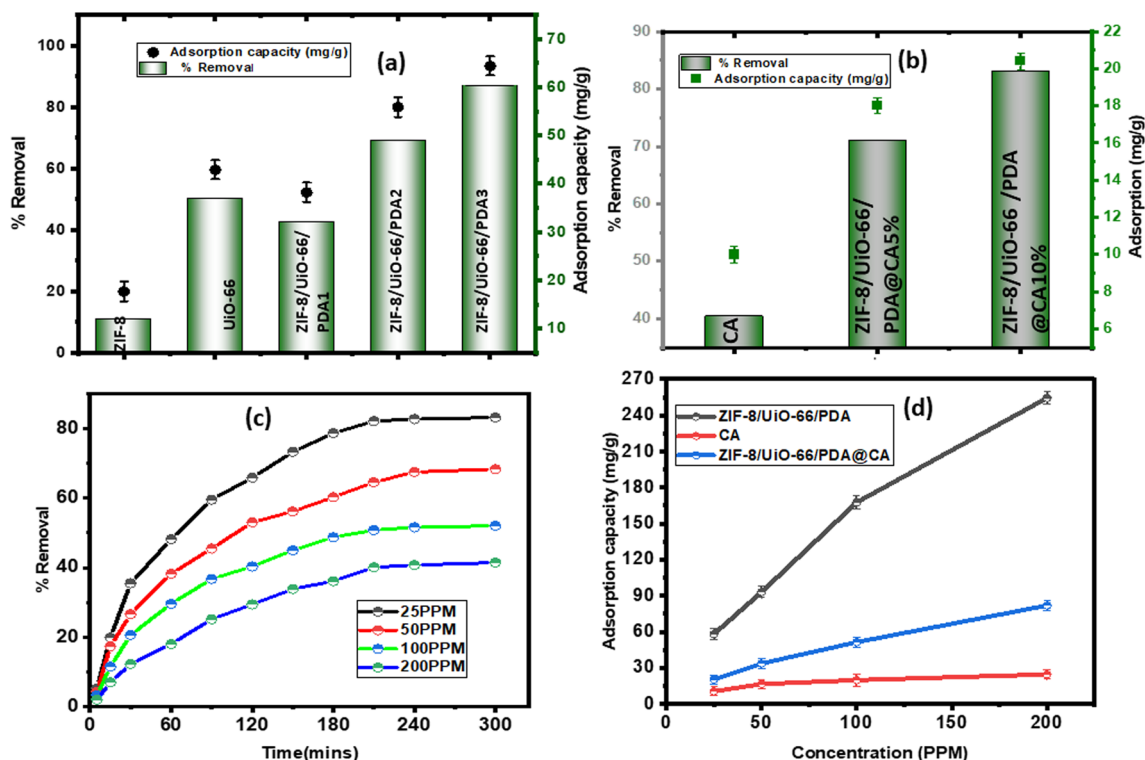


Fig. 7 **a** MOFs composites comparison. **b** Adsorption capacity of the fabricated ZIF-8/UiO-66/PDA@CA1, and ZIF-8/UiO-66/PDA@CA2 nanofibers **c** Effect of initial concentrations of MB on ZIF-8/UiO-66/

PDA@CA2 (pH 9, Temp. 25 °C, 0.05 g, Conc. 25 ppm). **d** Overall performance of CA, ZIF-8/UiO-66/PDA, and ZIF-8/UiO-66/PDA@CA2 nanofiber

Table 1 The mechanical properties of the fabricated ZIF-8/UiO-66/PDA@CA nanofiber

Samples	ZIF-8/UiO-66/PDA loading efficiency	Young modulus (MPa)	Tensile strength (MPa)	Elongation (%)
CA	0	45	1.0	4.0
ZIF-8/UiO-66/PDA@CA1	5%	131	2.8	2.0
ZIF-8/UiO-66/PDA@CA2	10%	122	2.2	1.0

outstanding performance might be due to the anionic surface of ZIF-8 as proposed by the zeta potential, and the successful transformation of the hydrophobic nature of ZIF-8 to hydrophilic enabling more dispersion of the MOF material in dye solution. It is interesting to note that the maximum adsorption capacity of ZIF-8/UiO-66/PDA was found to be 254 mg/g; the increase in performance over the single parent MOFs might be projected by the many catechol groups of PDA, which formed an ionic bond with MB.

Performance of the nanofibers toward MB dye removal

To reach the best material for MB removal, CA nanofiber, ZIF-8/UiO-66/PDA@CA1, and ZIF-8/UiO-66/PDA@CA2 nanofibers (Fig. 7b) were compared under optimum conditions (at constant pH 9, Temp. 25 °C, 0.05 g, and Conc. 25 ppm). The results suggested that ZIF-8/UiO-66/PDA@

CA1 nanofibers were comparatively better for the removal of MB over CA nanofiber (41%) due to the presence of MOFs in the matrix. It was also observed that removal increases (70–85%) with increasing the amount of MOF composite in the nanofiber (ZIF-8/UiO-66/PDA2). The corresponding adsorption capacity for CA, ZIF-8/UiO-66/PDA@CA1, and ZIF-8/UiO-66/PDA@CA2 were found to be 9.25, 15.4, and 21 mg/g, respectively.

Factor affecting the adsorption processes

Effect of contact time Decolorization of ZIF-8/UiO-66/PDA@CA2 nanofiber from an aqueous solution was investigated at different time intervals to attain the maximum adsorption by the ZIF-8/UiO-66/PDA@CA2 nanofiber (Fig. 7c) at a given time. Adsorption was monitored for 300 min (at constant pH 9, Temp. 25 °C, adsorbent dose

0.05 g, and Conc. 25–200 ppm), and it clearly showed the significant removal of MB by ZIF-8/UiO-66/PDA@CA2 nanofiber with time and was found to attend equilibrium at 180 min with an adsorption capacity of 76.1 mg/g. The diffusion of dye was made easy due to the smaller diameter of the porous spun fibers and the availability of the abundant vacant sites of the adsorbent at the initial time of adsorption.

The effect of initial dye concentration The adsorption is greatly influenced by the concentration of the analyte (Fig. 7d). The adsorption of MB onto ZIF-8/UiO-66/PDA@CA2 nanofiber surface was studied at a different initial concentration ranging from 25 to 200 mg L⁻¹ (at constant contact time 180 min, pH 9, Temp. 25 °C, and adsorbent dose 0.05 g). The dye adsorption capacities onto adsorbent increased with the increase in the concentration of dye solutions, and the maximum adsorption capacities for ZIF-8/UiO-66/PDA@CA2 nanofiber reached 82 mg g⁻¹, which is higher than the pristine CA with 22.4 mg/g (Fig. 7d). It was observed that the overall removal efficiency of dyes declined slightly with a rise in initial dye concentration; this may be due to insufficient vacant active sites to occupy the dye molecules at the saturation stage and so shows decrease in further removal of MB onto ZIF-8/UiO-66/PDA@CA2 nanofiber from aqueous phase (Li et al. 2020).

Complex purification performance Other typical contaminants (such as dyes) frequently coexist in complicated wastewater. In such a complicated system, most separating membranes were inefficient at eliminating concurrent pollutants and quickly fouled. Therefore, it was necessary to evaluate the ZIF-8/UiO-66/PDA@CA nanofiber's adsorption ability towards MB in the presence of interfering anionic dye (CR) and cationic dye (CV). In the single system, about 83 and 58% of MB and CR dye were removed, respectively (Fig. 8).

While in the binary system, about 72 and 90% of MB/CV and MB/CR were removed, respectively. The elimination (%) of CR over MB dyes has significantly decreased, which reflects the selectivity of ZIF-8/UiO-66/PDA@CA nanofibers towards MB. The removal (%) does, however, increase to 90% in the binary system of MB/CR compared to a binary system of CV/MB dye with 73%, which is most likely because the few positive charges present in the composite fully participated through their interaction with anionic CR dye. The decrease in the removal value in the binary system of MB/CV could be due to dyes competing fiercely for the adsorbent's active sites and might also have interacted with one another. The overall adsorption capacity is 82, 43, 70, and 108 mg/g for MB, CR, binary MB/CV, and binary MB/CR, respectively.

The effect of pH on adsorption The pH of the solution is a necessary parameter to consider during the adsorption process, as it influences the degree of ionization of the dye (Li et al. 2020). The adsorption of dye onto ZIF-8/UiO-66/PDA@CA2 nanofiber was studied at different pHs to ascertain the optimum pH for maximum adsorption (at constant contact time 180 min, vol. 50 mL, Temp. 25 °C, adsorbent dose 0.05 g, and Conc. 50 ppm). It was found that adsorption increases from 37 to 83% as the pH moves from pH=3 to pH=10, showing maximum adsorption capacity (20.4 mg/g) at alkaline medium) as shown in Fig. 9a. The performance of ZIF-8/UiO-66/PDA@CA2 nanofiber composite was greater in alkaline medium, because in alkaline medium, the adsorbent surface becomes deprotonated creating more negative charges and increasing the available site for interaction between the cationic dye and ZIF-8/UiO-66/PDA@CA nanofiber (Hakro et al. 2021). However, decreasing the pH causes a decrease in removal efficiency; this is due to the positively charged ions formed during protonation of

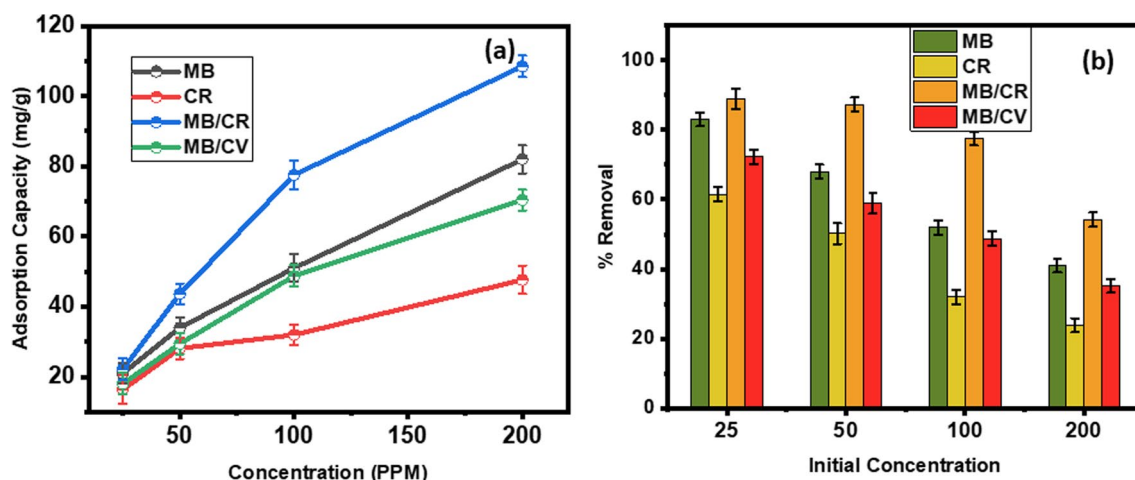


Fig. 8 Performance of ZIF-8/UiO-66/PDA@CA nanofibers in complex wastewater

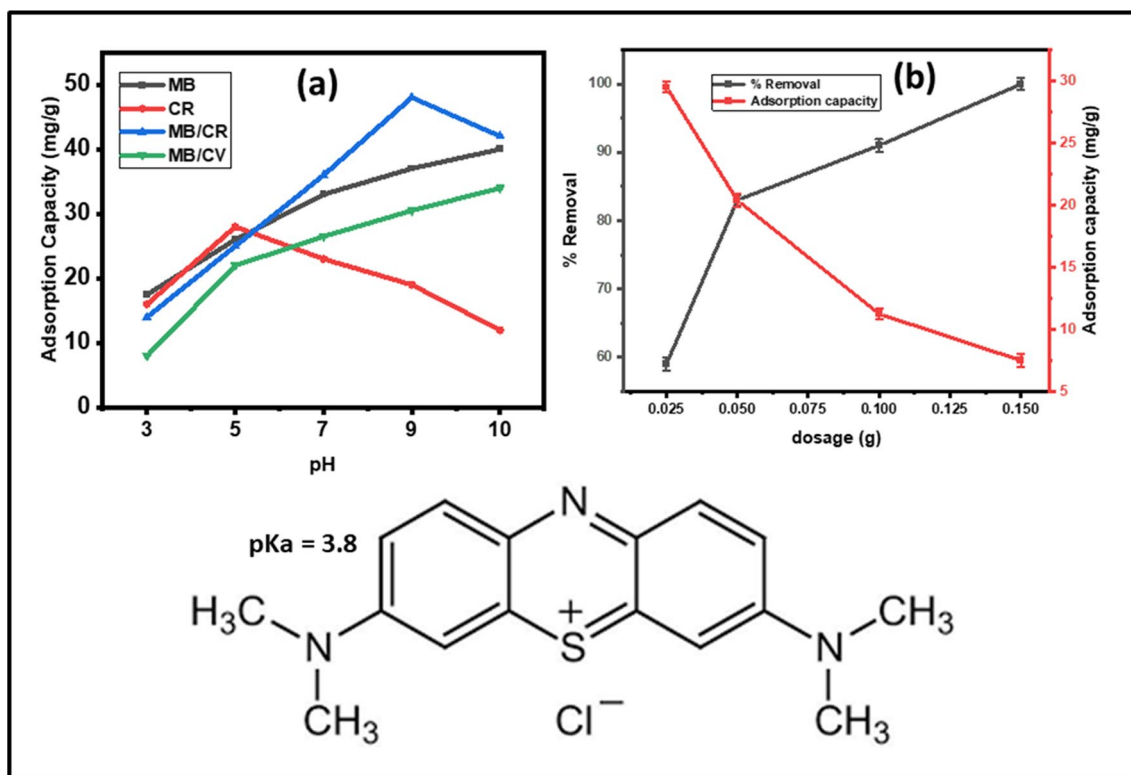


Fig. 9 Effect of pH (a) and adsorbent dosage (b) on the removal of MB by ZIF-8/UiO-66/PDA@CA2 nanofiber [$V=50$ mL, $T=25$ °C, $m=0.05$ g, $[C]_0=50$ ppm)

the carboxylic and amino group in ZIF-8/UiO-66/PDA nanofiber which causes electrostatic repulsion between adsorbent surface and dye solution, and increases competes between proton and MB for the available site (Li et al. 2020). CR shows maximum adsorption in the acidic medium due to protonation which causes more positive charge needed to interact with the anionic CR dye, and a reduction in the number of anions competing for adsorbent site. MB/CV shows the same trend as MB while the MB/CR gives maximum adsorption at pH 9 beyond this point a sharp decrease was observed which is due to numerous anions competing with CR for the adsorption site.

Effect of adsorbent dose The effect of ZIF-8/UiO-66/PDA@CA nanofiber dosage on MB removal (%) was demonstrated in Fig. 9b. It is evident from the curve that the MB removal performance increases with adsorbent dosage (at constant contact time 180 min, vol. 50 mL, Temp. 25 °C, and Conc. 50 ppm). The percentage uptake increases (59–100%) with an increase in the adsorbent dose of (0.025–0.15 g) on the contrary the adsorption capacity decreases from 29 to 7.5 mg/g due to an increase in unoccupied vacant sites and surface area

of the examined ZIF-8/UiO-66/PDA@CA2 nanofiber adsorbent as the dosage increases (Hakro et al. 2021).

Kinetics study

Pseudo-first order and -second order were applied to study the kinetics and expressed adsorption rate and mechanisms of MB onto ZIF-8/UiO-66/PDA@CA nanofiber (Fig. S3). The pseudo-first order is chemically inclined and is represented by Eq. 3 (Omer et al. 2020):

$$\ln(q_e - q_t) = \ln q_e - K_1 t \quad (3)$$

where q_t represents the adsorption capacity (mg/g) at time t , while K_1 (min^{-1}) is the equilibrium rate constant. Pseudo-second order is physically inclined and is represented in Eq. 4:

$$\frac{t}{q_e} = \frac{1}{K_2 q_e^2} + \frac{1}{q_e} \quad (4)$$

From the obtained values (Table 2), both pseudo-first and -second models were suitable for the reaction with the R^2 value close to 1. However, PSO best fits the adsorption

Table 2 The obtained parameters from PFO and PSO kinetic models for the adsorption MB by ZIF-8/UiO-66/PDA@CA2 nanofiber

Kinetic models and parameter			Initial	Concentration
	25	50	100	200
qe (mg/g)	20.4	33.7	51.3	81.9
Pseudo-first order				
qe (mg/g)	23.1	29.0	48.2	96.5
K_1	0.00019	0.00012	0.00011	0.00014
R^2	0.953	0.986	0.978	0.888
Pseudo-second order				
qe (mg/g)	25	40	66.66	90.9
K_1	0.00473	0.00088	0.000471	0.000341
R^2	0.994	0.993	0.994	0.976

process, and therefore, the rate-determining step is chemical sorption (Omer et al. 2019; Liang et al. 2019).

Adsorption isotherms

To study the form of interaction between MB and the synthesized ZIF-8/UiO-66/PDA@CA nanofiber, Langmuir, and Freundlich isotherm (Fig. S4) were adopted to explain the equilibrium adsorption characteristics, and the value of R is used to predict the most fitted model. Equation 5 represents Langmuir’s isotherm (Morcos et al. 2021).

$$\frac{C_e}{q_e} = \frac{1}{q_m K_L} + \frac{C_e}{q_m} \tag{5}$$

where q_{max} represents the maximum adsorption capacity (mg/g) and K_L (L/mg) is Langmuir’s isotherm constant which shows the binding affinity between MB and the ZIF-8/UiO-66/PDA@CA nanofiber. The separation factor (R_f) was calculated using Eq. 6 (Omer et al. 2019; Liang et al. 2019; Eltaweil et al. 2020a, b).

$$R_L = \frac{1}{1 + Ci \times K_L} \tag{6}$$

$$qe = K_f C_e \frac{1}{n} \tag{7}$$

$$\log q_e = \log K_f + \frac{1}{n} \log C_e \tag{8}$$

Freundlich’s model is represented by Eqs. 7 and 8. The constant “k” measures the adsorption capacity, while the intensity of adsorption is represented by 1/n. The value of 1/n is used to demonstrate if the adsorption process is favorable ($0.1 < 1/n < 0.5$) or unfavorable ($1/n > 2$) (Asif and Rafique 2021; Lee et al. 2015). From the isotherm plot and their derived parameter demonstrated in Table 3, both Langmuir and Freundlich’s isotherm fitted well for

Table 3 Parameters of isotherm models for the adsorption MB by ZIF-8/UiO-66/PDA@CA2 nanofiber

Isotherm	Parameter	Value
Langmuir	q_m (mg/g)	76.90
	K_L	0.0132
	R^2	0.999
Freundlich	K_F (L/mg)	9.44
	1/n	2.46
	R^2	0.9703
Temkin	B (Jmol ⁻¹)	19.90
	R^2	0.964
	K_T (L mg ⁻¹)	4.10

the reaction process. However, R_L (0.9991) of Langmuir is higher than that of Freundlich linear regression isotherm ($R_L = 0.9703$); therefore, Langmuir best describes the process of reaction. The derived n value from the Langmuir model (0.999) also suggests monolayer adsorption. The R -value was less than unity which indicates that this model is suitable for this process.

Furthermore, Temkin’s isotherm expressed the relationship between the adsorbed MB per gram of ZIF-8/UiO-66/PDA@CA2 nanofiber. The Temkin model states that the adsorption heat of all molecules decreases as the coverage of the adsorbent surface increases. The model is expressed in Eq. 9 and linearized in Eq. 10 (Vadi et al. 2013 and Khan et al. 2022):

$$Q_e = \frac{RT}{b} \text{LN}(KTC_e) \tag{9}$$

$$q_e = B \ln K_T + B \ln C_e \tag{10}$$

where B is the Temkin’s constant, K_T is the binding energy, and by plotting q_e against $\ln C_e$, the constant and other parameters listed in Table 3 can be calculated. From the calculated data displayed in Table 3, the R^2 value of Temkin shows the model is suitable for

explaining the adsorption process. Temkin constant (0.311 kJmol) is less than unity which shows that physical adsorption might have occurred (Vadi et al. 2013 and Khan et al. 2022). However, the heat of adsorption proves that the form of interaction is through physical and chemical forces.

Adsorption mechanism

The ZIF-8/UiO-66/PDA@CA nanofiber interaction and adsorption mechanisms were analyzed by XPS before (Fig. 4) and after (Fig. 10) adsorption to identify the type of interaction that occurs between ZIF-8/UiO-66/PDA@CA2 nanofiber and MB. The XPS C1s spectrum peaks at 290 eV which is ascribed to C=O–O peaks shows an increase in intensity after adsorption with a shift to higher energy which might have resulted from the interaction of the (COO⁻) and positively charged (CH₃)₂NH₂⁺ of MB through electrostatic interaction. Hydrogen bonding is also suspected to have occurred. The peaks at 284.9 eV allocated to C–C intensified which may be resulting from the added atoms of C–C and C–H of MB. A provoked projection was observed for N1s at 401 and 399 eV which depicts NH and NH₂. The projection of this peak is suspected to have resulted from added NH₂⁺ of MB and maybe electrostatic attraction between the (CH₃)₂NH₂⁺

of MB and the NH⁻ of the adsorbent (Fig. 11). The O1s spectrum showed new peaks at 536 eV which represent chemically adsorbed water molecule from the dye solution (Ganguly et al. 2011; Franciski et al. 2018). The OH peaks of O1s were also intensified because of hydrogen bonding between the oxygen groups of ZIF-8/UiO-66/PDA@CA2 nanofiber and the (CH₃)₂NH₂⁺ group of MB (Figs. 10 and 11). The survey further shows all characteristic peaks of both adsorbate and adsorbent. No obvious changes in the peak's positions were observed at Zn2p spectra but the intensity increases almost 1/3 of the original peaks before adsorption which may be due to the interaction of the MB(-S(CH₂)₃) and positively charge center of ZnO (ZnOH⁺) (Feng et al. 2016). The Zr3d shows an intense peak at 181.5 eV and a shift in binding energy from the previous 188 eV belonging to (ZrO) to a lower binding energy of 186 eV. A change to the lower binding energy is believed to have resulted from a change in the oxidation state of zirconium from +4 to a lower oxidation state (+3) (Muneshwar and Cadien 2018; Bespalov et al. 2015).

Regeneration test

The reusability of the adsorbent ZIF-8/UiO-66/PDA@CA2 nanofiber was investigated for economical gain

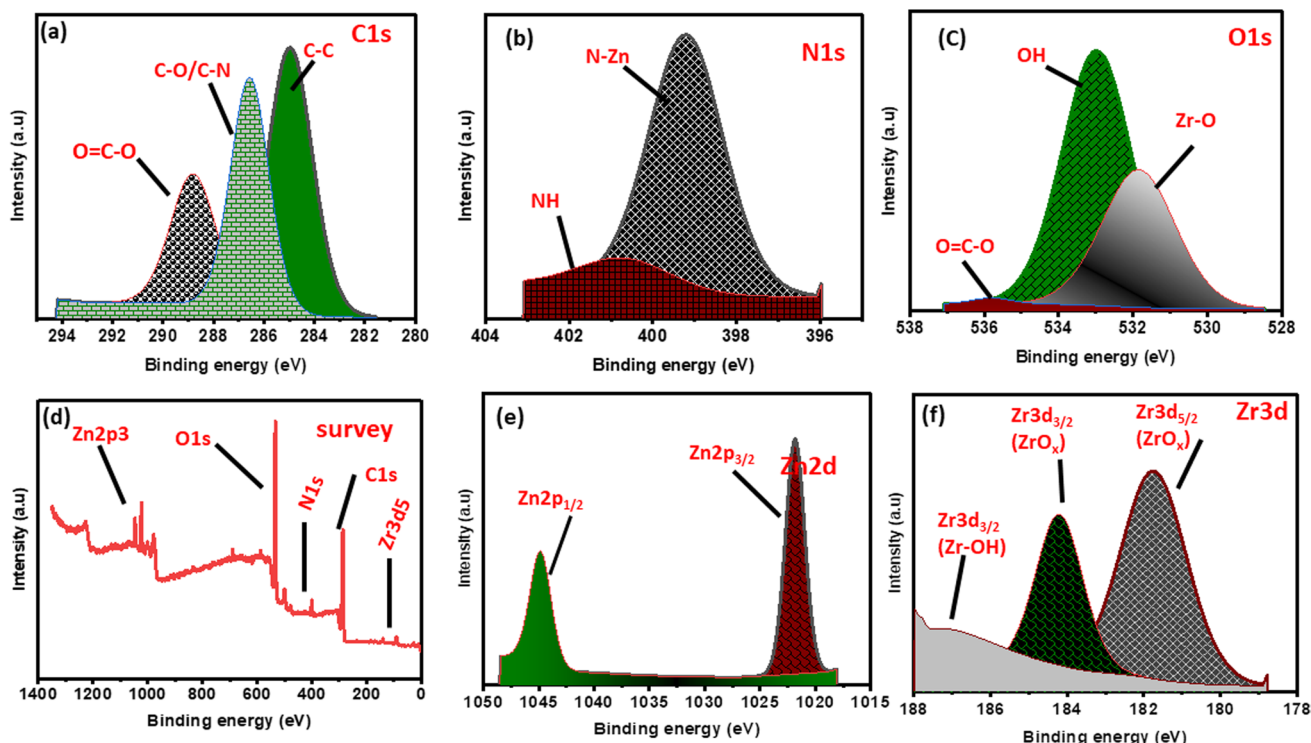


Fig. 10 XPS of ZIF-8/UiO-66/PDA@CA2 nanofiber after adsorption. **a** C1s, **b** N1s, **c** O1s, **d** survey, **e** Zn2p, and **f** Zr3

Fig. 11 Proposed adsorption mechanisms of MB onto ZIF-8/UiO-66/PDA@CA2 nanofiber

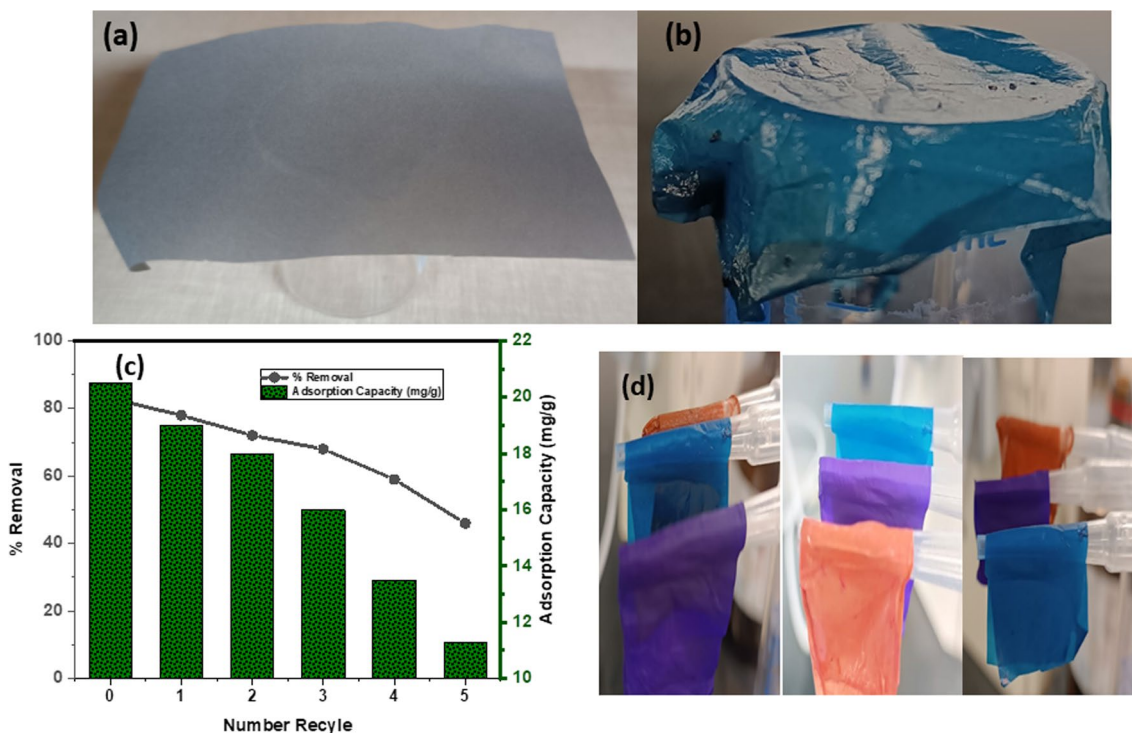
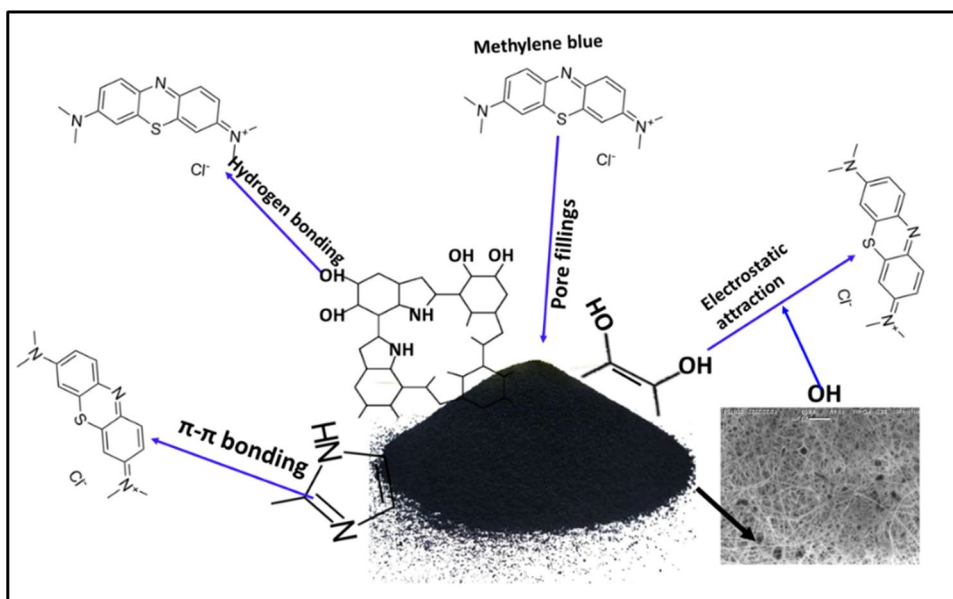


Fig. 12 ZiF-8/UiO-66/PDA@CA nanofiber **a** before adsorption and **b** after adsorption, and **c** number of recycle

(Fig. 12c). Water, diluted ethanol, and HCL were used as co-solvents to successfully regenerate the adsorbent ZIF-8/UiO-66/PDA@CA2 nanofiber. The performance is astounding from the first to the fifth cycle. The elimination percentage falls from 78 to 45%, while the adsorption capacity falls from 19.5 to 11.7 mg/g at the same time.

Comparison test

The fabricated ZIF-8/UiO-66/PDA@CA2 composite nanofiber was compared with other nanocomposites for MB adsorption performance (Table 4). The ZIF-8/UiO-66/PDA@CA2 nanofiber showed a more favorable capacity for MB adsorption.

Table 4 Comparison table of ZIF-8/Uio-66/PDA@CA2 nanofiber and other composite nanofiber towards adsorption of MB

Adsorbent	q_e (mg/g)	Time (min)	Reference
Spun PAN/PVDF membrane	30	15	Paclijan et al. 2021
Bio-MOFs@PAN	31	45	Li et al. 2020
Eu-MOF/CA	16	80	Mirhosseini et al. 2021
Pectin membrane	17	90	Hastuti et al. 2020
Polyniline/ β -cyclodextrin nanofiber	55	50	Ali et al. 2019
Acrylonitrile/CU-BTC	68	110	Wang et al. 2014
PDA/CA	80	1440	Cheng et al. 2020
rC/AC-EDTA	70	120	Elmaghraby et al. 2023
ZIF-8/Uio-66/PDA@CA2 nanofiber	82	180	This work

Conclusion

In summary, polydopamine polymerized binary MOFs were successfully used to fabricate ZIF-8/Uio-66/PDA composite. The fabricated ZIF-8/Uio-66/PDA composite was fully characterized and when examined for MB dye removal, a high efficiency towards removal of MB dye from an aqueous solution was achieved at a shorter time. Under optimum ZIF-8/Uio-66/PDA@CA nanofiber was successfully fabricated through electrospinning with different loading of ZIF-8/Uio-66/PDA. The fabricated ZIF-8/Uio-66/PDA@CA1 exhibited the highest stability after the mechanical test over ZIF-8/Uio-66/PDA@CA2 and CA nanofiber. After the performance test for dye removal. ZIF-8/Uio-66/PDA expressed an adsorption capacity of 254 mg/g higher than the parent MOFs. ZIF-8/Uio-66/PDA@CA2 nanofiber expressed maximum adsorption of 82 mg/g higher than the pristine CA with 22.4 mg/g. For the binary system, a maximum adsorption capacity of 70 and 108 mg/g was recorded for MB/CV and MB/CR. The adsorption studies favor Langmuir and pseudo-second order. The reproducibility/durability of the fabricated nanofiber over five consecutive times was achieved. These unique properties render it a promising durable adsorbent for the efficient removal of noxious methylene dye. These developed membranes can be an excellent solution for the textile industry, as one of most world's polluting industries.

Supplementary Information The online version contains supplementary material available at <https://doi.org/10.1007/s11356-024-33050-1>.

Acknowledgements Esther Eze would like to express gratitude to Tokyo International Conference on African Development (TICAD) for the scholarship. Ahmed Hassanin acknowledges Science, Technology & Innovation Funding Authority (STIFA), Egypt, Project 33431 DDP for supporting the manufacturing of all the nanofiber samples on the project's devices.

Author contribution Esther Eze: fabrication and characterization of the materials, running the experiments for adsorption of MB, writing the

manuscript. Ahmed M. Omer: conceptualization, data analysis, writing the manuscript, and supervision. Ahmed Hassanin: methodology for fabrication of nanofiber, and supervision. Abdelazeem S. Eltaweil: conceptualization, methodology, writing the manuscript, and supervision. Mohamed E. El-Khouly: conceptualization, fabrication, and characterization of the materials, editing the manuscript, and supervision.

Declarations

Ethics approval Not applicable.

Consent to participate Not applicable.

Consent for publication Not applicable.

Conflict of interest The authors declare no competing interests.

References

- Abd El-Monaem EM, Omer AM, Khalifa RE, Eltaweil AS (2022) Floatable cellulose acetate beads embedded with flower-like zwitterionic binary MOF/PDA for efficient removal of tetracycline. *J Colloid Interface Sci* 620:333–345
- Abdelfatah AM, Fawzy M, El-Khouly ME, Eltaweil AS (2021) Efficient adsorptive removal of tetracycline from aqueous solution using phytosynthesized nano-zero valent iron. *J Saudi Chem Soc* 25:101365
- Ali ASM, El-Aassar MR, Hashem FS, Moussa NA (2019) Surface modified of cellulose acetate electrospun nanofibers by polyaniline/ β -cyclodextrin composite for removal of cationic dye from aqueous medium. *Fibers Polym* 20(10):2057–2069
- Ali Khan AS (2012) Evaluation of thermodynamic parameters of cadmium adsorption on sand from Temkin adsorption isotherm. *Turk J Chem* 36(3):437–443
- Asif I, Rafique U (2021) Cellulose acetate-based hybrid materials: fascinating material as a potential adsorbent for Congo red removal. *Desalin Water Treat* 244:302–324
- Ayiania M, Smith M, Hensley AJR, Scudiero L, McEwen JS, Garcia-Perez M (2020) Deconvoluting the XPS spectra for nitrogen-doped chars: an analysis from first principles. *Carbon* 162:528–544
- Bespalov I, Datler M, Buhr S, Drachsel W, Rupprechter G, Suchorski Y (2015) Initial stages of oxide formation on the Zr surface at low oxygen pressure: an in situ FIM and XPS study. *Ultramicroscopy* 159:147–151
- Chang PH, Lee YT, Peng CH (2020) Synthesis and characterization of hybrid metal zeolitic imidazolate framework membrane for efficient H₂/CO₂ gas separation. *Materials* 13(21):1–15

- Chen J, Li J, Zhan X, Han X, Chen C (2010) Effect of PEG additives on properties and morphologies of polyetherimide membranes prepared by phase inversion. *Front Chem Eng China* 4(3):300–306
- Chen Q, He Q, Lv M, Xu Y, Yang H, Liu X, Wei F (2015) Selective adsorption of cationic dyes by UiO-66-NH₂. *Appl Surf Sci* 327:77–85
- Chen R, Lin B, Luo R (2022) Recent progress in polydopamine-based composites for the adsorption and degradation of industrial wastewater treatment. *Heliyon* 8(12):e12105
- Cheng J, Zhan C, Wu J, Cui Z, Si J, Wang Q, Peng X, Turng LS (2020) Highly efficient removal of methylene blue dye from an aqueous solution using cellulose acetate nanofibrous membranes modified by polydopamine. *ACS Omega* 5(10):5389–5400
- Ding M, Cai X, Jiang HL (2019) Improving MOF stability: approaches and applications. *Chem Sci* 10(44):10209–10230
- Elmaghraby NA, Omer AM, Kenawy ER, Gaber M, El Nemr A (2022) Electrospun composites nanofibers from cellulose acetate/carbon black as efficient adsorbents for heavy and light machine oil from aquatic environment. *J Iran Chem Soc* 19(7):3013–3027
- Elmaghraby NA, Omer AM, Kenawy ER, Gaber M, Hassaan MA, Ragab S, Hossain I, Nemr AE (2023) Electrospun cellulose acetate/activated carbon composite modified by EDTA (rC / AC - EDTA) for efficient methylene blue dye removal. *Sci Rep* 13:19919
- Eltaweil AS, Abd El-Monaem EM, El-Subruiti GM, Abd El-Latif MM, Omer AM (2020a) Fabrication of UiO-66/MIL-101(Fe) binary MOF/carboxylated-GO composite for adsorptive removal of methylene blue dye from aqueous solutions. *RSC Adv* 10(32):19008–19019
- Eltaweil AS, Elgarhy GS, El-Subruiti GM, Omer AM (2020b) Carboxymethyl cellulose/carboxylated graphene oxide composite microbeads for efficient adsorption of cationic methylene blue dye. *Int J Biol Macromol* 154:307–318
- Eze E, Omer AM, Hassanin AH, Eltaweil AS, El-Khouly ME (2023) Efficient removal of noxious methylene dye by low-cost and reusable composite beads based on cellulose acetate/banana pseudostem fiber. *Biomass Conversion and Biorefinery*, in press
- Fendi W, Naser J (2018) Adsorption isotherms study of methylene blue dye on membranes from electrospun nanofibers. *Orient J Chem* 34(6):2884–2894
- Feng Y, Li Y, Xu M, Liu S, Yao J (2016) Fast adsorption of methyl blue on zeolitic imidazolate framework-8 and its adsorption mechanism. *RSC Adv* 6(111):109608–109612
- Franciski MA, Peres EC, Godinho M, Perondi D, Foletto EL, Collazzo GC, Dotto GL (2018) Development of CO₂ activated biochar from solid wastes of a beer industry and its application for methylene blue adsorption. *Waste Manage* 78:630–638
- Ganguly A, Sharma S, Papakonstantinou P, Hamilton J (2011) Probing the thermal deoxygenation of graphene oxide using high-resolution in situ X-ray-based spectroscopies. *J Phys Chem C* 115(34):17009–17019
- Gondal MA, Fasasi TA, Baig U, Mekki A (2017) Effects of oxidizing media on the composition, morphology and optical properties of colloidal zirconium oxide nanoparticles synthesized via pulsed laser ablation in liquid technique. *J Nanosci Nanotechnol* 18(6):4030–4039
- Gopi S, Pius A, Kargl R, Kleinschek KS, Thomas S (2019) Fabrication of cellulose acetate/chitosan blend films as efficient adsorbent for anionic water pollutants. *Polym Bull* 76(3):1557–1571
- Hakro RA, Mehdi M, Qureshi RF, Mahar RB, Khatri M, Ahmed F, Khatri Z, Kim IS (2021) Efficient removal of reactive blue-19 dye by co-electrospun nanofibers. *Mater Res Express* 8(5):1–11
- Hastuti B, Nur Afifah S, Mulyani B, Susilowati E (2020) Adsorption of methylene blue dyes using pectin membrane. *J Phys Confer Ser* 1503 (1)
- Katz MJ, Brown ZJ, Colón YJ, Siu PW, Scheidt KA, Snurr RQ, Hupp JT, Farha OK (2013) A facile synthesis of UiO-66, UiO-67 and their derivatives. *Chem Commun* 49(82):9449–9451
- Khan I, Saeed K, Zekker I, Zhang B, Hendi AH, Ahmad A, Khan I (2022) Review on methylene blue: its properties, uses, toxicity and photodegradation. *Water* 14(2):242
- Kim EY, Kim HS, Kim D, Kim J, Lee PS (2019) Preparation of mixed matrix membranes containing ZIF-8 and UiO-66 for multicomponent light gas separation. *Crystals* 9(1):15
- Koriam OA, Kamel AM, Shaaban W, Elkady MF (2022) Enhancement of dye separation performance of eco-friendly cellulose acetate-based membranes. *Sustainability* 14(22):14665
- Lee YR, Jang MS, Cho HY, Kwon HJ, Kim S, Ahn WS (2015) ZIF-8: a comparison of synthesis methods. *Chem Eng J* 271:276–280
- Li Y, Zhou K, He M, Yao J (2016) Synthesis of ZIF-8 and ZIF-67 using mixed-base and their dye adsorption. *Microporous Mesoporous Mater* 234:287–292
- Li T, Liu L, Zhang Z, Han Z (2020) Preparation of nanofibrous metal-organic framework filter for rapid adsorption and selective separation of cationic dye from aqueous solution. *Sep Purif Technol* 237:116360
- Liang XX, Omer AM, Hu Z, Wang Y, Yu D, Ouyang X (2019) Efficient adsorption of diclofenac sodium from aqueous solutions using magnetic amine-functionalized chitosan. *Chemosphere* 217:270–278
- Liebscher J (2019) Chemistry of polydopamine-scope, variation, and limitation. *Eur J Org Chem* 19(32):4976–4994
- Luan Tran B, Chin HY, Chang BK, Chiang AST (2019) Dye adsorption in ZIF-8: the importance of external surface area. *Microporous Mesoporous Mater* 277:149–153
- Mandal S, Natarajan S, Mani P, Pankajakshan A (2021) Post-synthetic modification of metal-organic frameworks toward applications. *Adv Func Mater* 31(4):2006291
- Mirhosseini H, Shamspur T, Mostafavi A, Sargazi G (2021) A novel ultrasonic reverse micelle-assisted electrospun efficient route for Eu-MOF and Eu-MOF/CA composite nanofibers: a high-performance photocatalytic treatment for removal of BG pollutant. *Environ Sci Pollut Res* 28(4):4317–4328
- Modi S, Yadav VK, Gacem A, Ali IH, Dave D, Khan SH, Yadav KK, Rather SU, Ahn Y, Son CT, Jeon BH (2022) Recent and emerging trends in remediation of methylene blue dye from wastewater by using zinc oxide nanoparticles. *Water* 14(11):1749
- Mohammadi AA, Alinejad A, Kamarehie B, Javan S, Ghaderpoury A, Ahmadpour M, Ghaderpoori M (2017) Metal-organic framework UiO-66 for adsorption of methylene blue dye from aqueous solutions. *Int J Environ Sci Technol* 14(9):1959–1968
- Mondal NK, Das K, Das B, Sadhukhan B (2016) Effective utilization of calcareous soil towards the removal of methylene blue from aqueous solution. *Clean Technol Environ Policy* 18(3):867–881
- Morcós GS, Ibrahim AA, El-Sayed MMH, El-Shall MS (2021) High performance functionalized UiO metal organic frameworks for the efficient and selective adsorption of Pb(II) ions in concentrated multi-ion systems. *J Env Chem Eng* 3:105191
- Muneshwar T, Cadien K (2018) Comparing XPS on bare and capped ZrN films grown by plasma enhanced ALD: effect of ambient oxidation. *Appl Surf Sci* 435:367–376
- Muqeet M, Khalique A, Qureshi UA, Mahar RB, Ahmed F, Khatri Z, Kim IS, Brohi KM (2018) Aqueous hardness removal by anionic functionalized electrospun cellulose nanofibers. *Cellulose* 25(10):5985–5997
- Omer AM, Khalifa RE, Hu Z, Zhang H, Liu C, Ouyang X (2019) Fabrication of tetraethylenepentamine functionalized alginate beads for adsorptive removal of Cr (VI) from aqueous solutions. *Int J Biol Macromol* 125:1221–1231
- Omer AM, Elgarhy GS, El-Subruiti GM, Khalifa RE, Eltaweil AS (2020) Fabrication of novel iminodiacetic acid-functionalized

- carboxymethyl cellulose microbeads for efficient removal of cationic crystal violet dye from aqueous solutions. *Int J Biol Macromol* 148:1072–1083
- Paclijan SS, Franco SMB, Abella RB, Lague JCH, Tan NPB (2021) Fresh and uncalcined solution blow spinning - spun PAN and PVDF nanofiber membranes for methylene blue dye removal in water. *J Membr Sci Res* 7(3):173–184
- Pi Y, Li X, Xia Q, Wu J, Li Y, Xiao J, Li Z (2018) Adsorptive and photocatalytic removal of Persistent Organic Pollutants (POPs) in water by metal-organic frameworks (MOFs). *Chem Eng J* 337:351–371
- Pottathara YB, Narwade VN, Bogle KA, Kokol V (2020) TEMPO-oxidized cellulose nanofibrils–graphene oxide composite films with improved dye adsorption properties. *Polym Bull* 77(12):6175–6189
- Ruan H, Pan N, Wang C, Yu L, Liao J, Shen J (2021) Functional UiO-66 series membranes with high perm selectivity of monovalent and bivalent anions for electrodialysis applications. *Ind Eng Chem Res* 60(10):4086–4096
- Sağlam S, Türk FN, Arslanoğlu H (2023) Use and applications of metal-organic frameworks (MOF) in dye adsorption. *J Environ Chem Eng* 11(5):110568
- Tag El-Din AF, El-Khouly ME, Elshehy EA, Atia AA, El-Said WA (2018) Cellulose acetate assisted synthesis of worm-shaped mesopores of MgP ion-exchanger for cesium ions removal from seawater. *Microporous Mesoporous Mater* 265:211–218
- Tang B, Wu D, Xu T (2005) Effect of PEG additives on properties and morphologies of membranes prepared from poly(2,6-dimethyl-1,4-phenylene oxide) by benzyl bromination and in situ amination. *J Appl Polym Sci* 98(6):2414–2421
- Vadi M, Mansoorabad AO, Mohammadi M, Rostami N (2013) Investigation of Langmuir, Freundlich and Temkin adsorption isotherm of tramadol by multi-wall carbon nanotube. *Asian J Chem* 25(10):5467–5469
- Večeř M, Pospíšil J (2012) Stability and rheology of aqueous suspensions. *Proc Eng* 42:1720–1725
- Wang Z, Wang J, Li M, Sun K, Liu CJ (2014) Three-dimensional printed acrylonitrile butadiene styrene framework coated with Cu-BTC metal-organic frameworks for the removal of methylene blue. *Sci Rep* 4:4–10
- Wee Lik H, Janssens Nikki, Sree Sreeprasanth P, Wiktor Christian, Gobechiya Elena, Fischer Roland A, Kirschhock Christine EA, Martens Johan A (2014) Local transformation of ZIF-8 powders and coatings into ZnO nanorods for photocatalytic application. *Nanoscale* 6(4):2056–2060
- Yang X, Zhou Y, Sun Z, Yang C, Tang D (2021) Polydopamine assists the continuous growth of zeolitic imidazolate framework-8 on electrospun polyacrylonitrile fibers as efficient adsorbents for the improved removal of Cr(vi). *New J Chem* 45(34):15503–15513
- Zha Q, Sang X, Liu D, Wang D, Shi G, Ni C (2019) Modification of hydrophilic amine-functionalized metal-organic frameworks to hydrophobic for dye adsorption. *J Solid State Chem* 275:23–29
- Zhang M, Yang K, Cui J, Yu H, Wang Y, Shan W, Lou Z, Xiong Y (2020) 3D-agaric like core-shell architecture UiO-66-NH₂@ZIF-8 with robust stability for highly efficient REEs recovery. *Chem Eng J* 386:124023
- Zhou HC, Long JR, Yaghi OM (2012) Introduction to metal-organic frameworks. *Chem Rev* 112(2):673–674

Publisher's Note Springer Nature remains neutral with regard to jurisdictional claims in published maps and institutional affiliations.

Springer Nature or its licensor (e.g. a society or other partner) holds exclusive rights to this article under a publishing agreement with the author(s) or other rightsholder(s); author self-archiving of the accepted manuscript version of this article is solely governed by the terms of such publishing agreement and applicable law.